Aging Cell (2010) **9,** pp761–775 Doi: 10.1111/j.1474-9726.2010.00609.x

Cyclophilin D links programmed cell death and organismal aging in *Podospora anserina*

Diana Brust,[1] Bertram Daum,[2] Christine Breunig,[1] Andrea Hamann,[1] Werner Kühlbrandt[2] and Heinz D. Osiewacz[1]

[1]Johann Wolfgang Goethe University, Faculty for Biosciences & Cluster of Excellence Macromolecular Complexes, Institute of Molecular Biosciences, Max-von-Laue-Street 9, 60438 Frankfurt, Germany

[2]Max Planck Institute of Biophysics, Department of Structural Biology, Max-von-Laue-Street 3, 60438 Frankfurt, Germany

Summary

Cyclophilin D (CYPD) is a mitochondrial peptidyl prolyl-*cis,trans*-isomerase involved in opening of the mitochondrial permeability transition pore (mPTP). CYPD abundance increases during aging in mammalian tissues and in the aging model organism *Podospora anserina*. Here, we show that treatment of the *P. anserina* wild-type with low concentrations of the cyclophilin inhibitor cyclosporin A (CSA) extends lifespan. Transgenic strains overexpressing *PaCypD* are characterized by reduced stress tolerance, suffer from pronounced mitochondrial dysfunction and are characterized by accelerated aging and induction of cell death. Treatment with CSA leads to correction of mitochondrial function and lifespan to that of the wild-type. In contrast, *PaCypD* deletion strains are not affected by CSA within the investigated concentration range and show increased resistance against inducers of oxidative stress and cell death. Our data provide a mechanistic link between programmed cell death (PCD) and organismal aging and bear implications for the potential use of CSA to intervene into biologic aging.

Key words: cell death; cyclophilin D; cyclosporin A; mitochondria; mPTP; *Podospora anserina*.

Introduction

Over the past few decades, a large body of data has accumulated to demonstrate a complex network of interacting pathways involved in the control of programmed cell death (PCD). In humans, impairments of the involved pathways lead to a variety of diseases including stroke, heart attack, autoimmune and neurodegenerative diseases as well as breast, colon, prostate and lung cancer (Zörnig *et al.*, 2001; Fadeel & Orrenius, 2005). In marked contrast, only little is known about the impact of PCD on aging. Here, we report our investigations of this particular issue in a genetically tractable short-lived aging model, the filamentous fungus *Podospora anserina*, which has a well-established mitochondrial etiology of aging (Osiewacz, 2002). Recently, in this system, extension of the healthy period of life, the healthspan, was reported as the result of genetic manipulation of molecular and cellular quality control systems involved in keeping a functional population of mitochondria for an extended period of time (Scheckhuber *et al.*, 2007; Luce & Osiewacz, 2009). Moreover, experimental evidence for PCD in this and other fungal systems has been reported (Hamann *et al.*, 2007, 2008; Brust *et al.*, 2009) and is currently under intense investigation. From these investigations, PCD emerges as part of the hierarchical and interconnected pathways involved in the control of lifespan and aging.

Here, we report investigations to unravel the role of PaCYPD in PCD and organismal aging. We selected PaCYPD for our studies because its level increases in *P. anserina* during aging (Groebe *et al.*, 2007), the sequence of cyclophilin D (CYPD) is conserved from yeast to humans (Fig. S1), and human CYPD is a known component of the mPTP (Grimm & Brdiczka, 2007; Kroemer *et al.*, 2007). This pore is thought to consist of outer and inner membrane proteins as well as proteins in the mitochondrial matrix. Although the structure and the regulation of the mitochondrial permeability transition pore are not finally established, it is widely accepted that the mitochondrial peptidyl prolyl-*cis,trans*-isomerase CYPD plays a key role in its regulation (Baines, 2009). Apart from a role in apoptosis (Liang & Zhou, 2007; Palma *et al.*, 2009), mammalian CYPD has recently been shown to bind to mitochondrial F_0F_1 ATPase and to regulate the activity of this mitochondrial protein complex (Giorgio *et al.*, 2009). In addition, CYPD was reported to be involved in another type of cell death that is highly controlled but also displays characteristics of necrosis (e.g. loss of membrane integrity, energy independence) and therefore was termed programmed necrosis (Golstein & Kroemer, 2007). Programmed necrosis can be blocked by the specific cyclophilin inhibitor cyclosporin A (CSA) emphasizing the involvement of CYPD and mPTP in this type of PCD (Zong & Thompson, 2006).

We show that the constitutive overexpression of *PaCypD* leads to a shortened lifespan of *P. anserina* and an early expression of apoptosis markers. CSA increases lifespan of wild-type strains and restores mitochondrial function and lifespan of *PaCypD* overexpressors. Overall, our study reveals mechanistic links

Correspondence
Heinz D. Osiewacz, Johann Wolfgang Goethe University, Faculty for Biosciences & Cluster of Excellence Macromolecular Complexes, Institute of Molecular Biosciences, Max-von-Laue-Str. 9, 60438 Frankfurt, Germany. Tel.: +49 69 79829263; fax: +49 69 79829363; e-mail:osiewacz@bio.uni-frankfurt.de

Accepted for publication *13 June 2010*

Aging Cell

between the aging process of *P. anserina* and the induction of PCD via the activation of the mPTP as the process bringing life of senescent strains to an end. PaCYPD, which can be inhibited by CSA, is a crucial component in this process. This finding identifies human CYPD as a promising target for interventions into aging via treatment with CSA which is an approved drug used as a human therapeutics.

Results

Increase in PaCYPD abundance accelerates aging

The earlier identification of increases in abundance of PaCYPD in purified mitochondria from senescent *P. anserina* cultures (Groebe *et al.*, 2007) prompted us to investigate the mechanistic role of this mitochondrial protein in aging and lifespan control. Toward this goal, we set out to modulate the abundance of the protein in the mitochondrial matrix by construction of both *PaCypD* deletion and overexpression strains. Deletion strains were generated via replacement of *PaCypD* by a bifunctional selection marker gene (Hamann *et al.*, 2005) (Fig. S2a,b). Overexpression strains were selected after introduction of a plasmid containing the *PaCypD* reading frame behind the strong constitutive basic *PaMt1* promoter of *P. anserina* into fungal spheroplasts of the wild-type strain 's' (Osiewacz *et al.*, 1991). Ectopic integration of the plasmid into the genome was verified by Southern blot analysis (Fig. S3a). At the transcript level, real-time PCR experiments demonstrated an 11- and 15-fold overexpression, respectively, of *PaCypD* in the two transgenic strains (*PaCypD*_OEx1 and *PaCypD*_OEx2) compared to the wild-type (Fig. S3b). Western blot analyses revealed the absence of PaCYPD in the deletion strain (Fig. 1a). PaCYPD levels were found to be 2.2- and 9.5-fold higher in senescent wild-type strains and 4-day-old *PaCypD* overexpressors, respectively, than in the juvenile wild-type (Fig. 1e). In contrast, abundance of the heat shock protein 60 (HSP60), a mitochondrial protein induced during stress, is not influenced by *PaCypD* overexpression, indicating that the strong overexpression of this gene does not lead to global mitochondrial impairments ('sickness') (Fig. S4).

Compared to the wild-type strain 's', lifespan, growth rate and fertility was not changed significantly in the deletion strain under standard growth conditions (Fig. 1b–d; Table S2, S4). Also, the characteristic accumulation of a circular DNA species (plDNA) in mitochondria, a robust molecular marker of wild-type-specific aging in *P. anserina* (Osiewacz & Esser, 1984), occurred at the same rate as in the wild-type strain (Fig. S2c). In marked contrast, in *PaCypD* overexpressing strains, the lifespan of both transgenic strains was strongly reduced. Reduction of the mean lifespan was 61% for strain *PaCypD*_OEx2 and 50% for strain *PaCypD*_OEx1 (Fig. 1f). The two strains were characterized by the accelerated expression of different senescence markers. The growth rate of *PaCypD*_OEx1 cultures was reduced by 17% and of *PaCypD*_OEx2 by 27.8% (Fig. 1g; Table S2, S4). The wild-type-specific reorganization of the mitochondrial DNA (mtDNA) occurred at an accelerated rate (Fig. S3c). Juvenile cultures of *PaCypD* overexpressors displayed impairments in female fertility. When spermatia (male gametes) from wild-type cultures or from the *PaCypD* overexpressing strain were used to fertilize ascogonia (female gametangia) of the opposite mating-type, normal fruiting bodies (perithecia) developed after 14 days of spermatization. In marked contrast, in reciprocal crosses in which ascogonia of the *PaCypD* overexpressing strain were fertilized by spermatia of the wild-type or *PaCypD*_OEx, no perithecia developed during this period of time. However, after 24 days of spermatization, some perithecia were found on these plates (Fig. 1h).

At the molecular level, juvenile *PaCypD* overexpressors displayed increased transcript levels of the metallothionein gene (*PaMt1*) and loss of superoxide dismutase 2 (PaSOD2) activity, two other senescence markers (Averbeck *et al.*, 2001; Borghouts *et al.*, 2002) in *P. anserina* (Fig. S5a–c).

Mitochondria of *PaCypD* overexpressing strains display premature senescence

In a next series of experiments, we analyzed the mitochondrial morphology of the strains. From previous analyses, it was known that mitochondria from juvenile wild-type strains are filamentous, while those from senescent strains are punctate (Scheckhuber *et al.*, 2007). Fluorescence microscopy of Mitotracker Red-stained mitochondria from the *PaCypD* overexpressors displayed a senescence-specific punctate structure. In contrast, in the deletion strain and in wild-type strain 's', mitochondria were filamentous (Fig. 2a).

Because PaCYPD, as a homolog of human CYPD, should interact with mitochondrial membrane complexes to form the mPTP, we next analyzed possible differences in mitochondrial ultrastructure of *P. anserina* in strains with different PaCYPD abundance by electron cryotomography. Comparing mitochondria of juvenile (6 days) and of senescent (20 days) wild-type strain cultures (Fig. 2b), we found that the fragile mitochondrial network of juvenile wild-type cultures had been fragmented during sample preparation. However, the fragments had resealed into mitochondria that were recognizably intact as they showed continuous outer and inner membranes, a narrow intermembrane space and a dense matrix. Most significantly, 75% of the mitochondria isolated from juvenile wild-type cultures displayed tubular or lamellar cristae extending into the matrix space (Fig. 2b). The cristae membrane surface exposed to the matrix had an overall convex curvature. The cristae junctions were slit-like, as appears to be characteristic for fungal mitochondria (Nicastro *et al.*, 2000). About 25% of the mitochondria isolated from juvenile wild-type cultures showed an unusual ultrastructure similar to the vesicular form described by others (Sun *et al.*, 2007). In these mitochondria, the cristae formed a continuous, reticulate network resembling a fishing net. Mitochondria isolated from senescent cultures likewise exhibited either the normal or the reticulate morphology. However, the proportion of both morphologies was the reverse of that in extracts of juvenile cultures. While 86% of the mitochondria had the reticulate

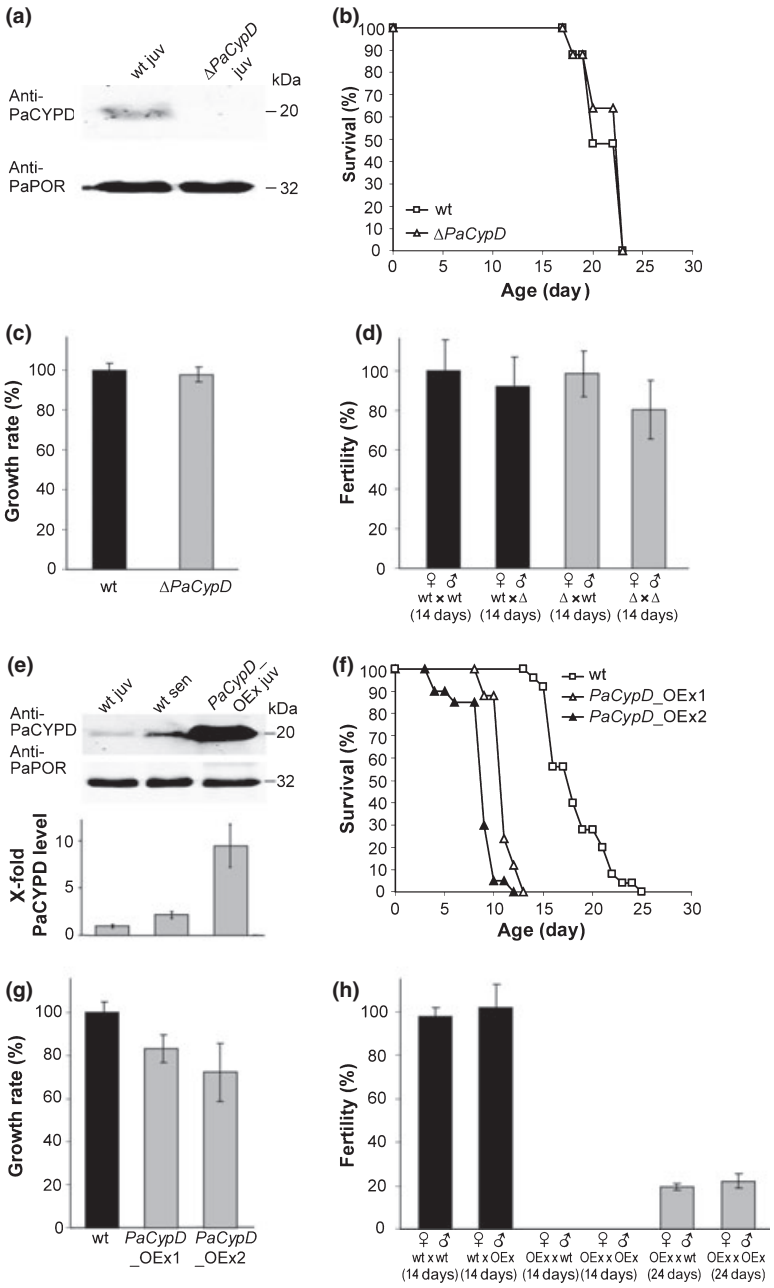

Fig. 1 Manipulation of *PaCypD* abundance. (a) Protein level of PaCYPD visualized by Western blot analysis using mitochondrial protein extracts from juvenile wild-type strain 's' and Δ*PaCypD*. Predicted sizes of the proteins are shown on the right. No PaCYPD was detected in mitochondria of the *PaCypD* deletion strain. PaPORIN (PaPOR) was used as loading control. (b) Mean lifespan of wild-type (21.2 ± 1.87; $n = 25$) and Δ*PaCypD* (21.68 ± 1.89; $n = 25$) grown on PASM ($P = 4E-1$). Lifespan of Δ*PaCypD* strains is comparable to wild-type lifespan. For verification, three additional statistical tests were performed (Table S2a). (c) Growth rate of wild-type (100 ± 3.3; $n = 25$) and of Δ*PaCypD* (97.7 ± 3.7; $n = 25$) grown on PASM ($P = 3.8E-1$). (d) Fertility of wild-type ($n = 10$) and Δ*PaCypD* ($n = 10$). Fertility of Δ*PaCypD* is unchanged in comparison with the wild-type strain 's' (wt × wt 100 ± 15.81; wt × Δ 92.23 ± 14.77, $P = 1.7E-1$; Δ × wt 98.42 ± 11.66, $P = 9E-1$; Δ × Δ 80.19 ± 14.72, $P = 1.1E-1$). (e) Protein level of PaCYPD visualized by Western blot analysis and densitometry using mitochondrial protein extracts from juvenile wild-type strain 's' ($n = 4$), senescent wild-type ($n = 4$) and juvenile *PaCypD*_OEx cultures ($n = 4$). Predicted sizes of the proteins are indicated on the right. Senescent wild-type mitochondria (2.19 ± 0.37; $P = 2.8E-2$) contain significantly more PaCYPD than juvenile wild-type mitochondria (1 ± 0.18). Juvenile *PaCypD*_OEx mitochondria show a strong increase in the level of PaCYPD (9.45 ± 2.27; $P = 2.8E-2$). PaPORIN was used as loading control for quantification. (f) Mean lifespan of *PaCypD*_OEx1 (11.12 ± 1.05; $n = 25$; $P = 1.42E-9$) and *PaCypD*_OEx2 (8.75 ± 1.94; $n = 20$; $P = 1.21E-8$) decrease strongly compared to wild-type strain 's' (18.82 ± 2.9; $n = 25$). (g) Growth rate of wild-type (100 ± 4.7; $n = 25$), *PaCypD*_OEx1 (83 ± 6.4; $n = 25$; $P = 4.14E-9$) and *PaCypD*_OEx2 (72.2 ± 13.4; $n = 20$; $P = 1.29E-8$) indicate a strongly reduced growth rate in the overexpressing strains. Three additional statistical tests demonstrate that the lifespan changes are significant (Table S2b). (h) Fertility of wild-type ($n = 10$) and *PaCypD*_OEx ($n = 10$). The *PaCypD* overexpressing strain is severely impaired in female fertility. Fruiting bodies of crosses in which the female partner is the wild-type strain develop in large numbers 14 days after fertilization. By contrast, only few fruiting bodies developed 24 days after fertilization when the female partner was the *PaCypD* overexpressing strain (wt × wt (14 d) 100 ± 6.73; wt × OEx (14 d) 104.05 ± 10.54, $P = 8.2E-1$; OEx × wt (24 d) 19.67 ± 1.63, $P = 1.8E-4$; OEx × OEx (24 d) 22.51 ± 3.34, $P = 1.8E-4$).

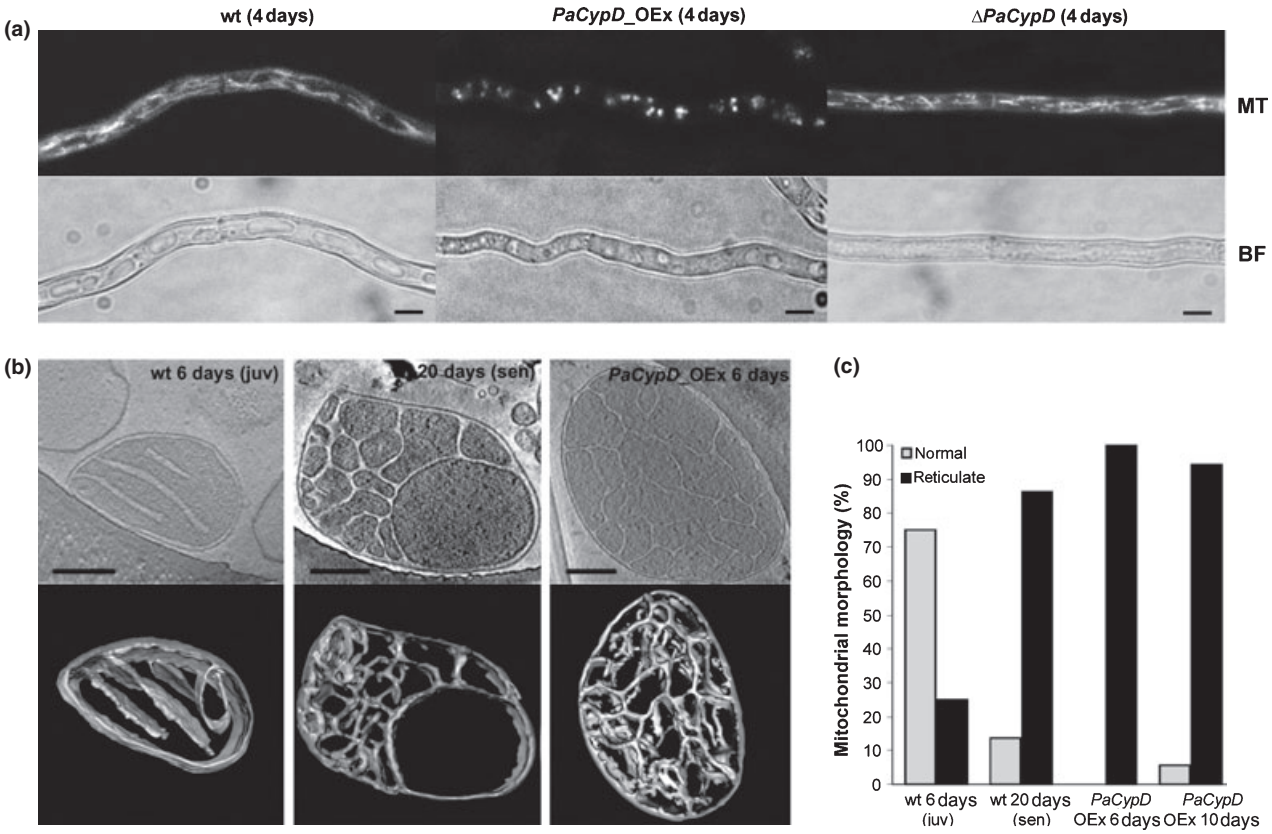

Fig. 2 Effect of PaCYPD on mitochondrial morphology. (a) Representative 4-day-old hyphae (BF: bright field) and mitochondria (MT: Mitotracker Red CMXRos) from wild-type strain 's', *PaCypD*_OEx and Δ*PaCypD* strains. Scale bars: 2 μm. Long, mitochondrial filaments are detected in wild-type and Δ*PaCypD*, while mitochondria are fragmented in *PaCypD*_OEx. (b) Mitochondrial ultrastructure revealed by electron cryotomography. Tomographic sections (upper row) and rendered volumes (lower row) of isolated mitochondria from juvenile (6 d) and senescent (20 d) wild-type 's' strain, and from 6-day-old *PaCypD*_OEx. Mitochondria from juvenile wild-type cultures display tubular or lamellar cristae, while the cristae of senescent wild-type strains and 6-day-old, prematurely aged *PaCypD* overexpressors form a continuous reticulate network with multiple branches. Scale bars: 200 nm. (c) Quantification of tubular and reticulate cristae formation in juvenile (6 d) wild-type (n = 24), senescent (20 d) wild-type (n = 22), presenescent (6 d) *PaCypD*_OEx (n = 25) and senescent (10 d) *PaCypD*_OEx (n = 18). Almost 100% of *PaCypD*_OEx mitochondria show the characteristic reticulate ultrastructure.

morphology, only 14% exhibited the normal morphology, indicating a drastic change in ultrastructure during aging. Reticulate mitochondria thus represent another senescence marker in *P. anserina*. Most significantly, mitochondria from 6-day-old cultures of *PaCypD* overexpressors did not show any significant difference to mitochondria prepared from senescent wild-type cultures (Fig. 2b). In *PaCypD*_OEx, almost 100% of the mitochondria were of the reticulate type (Fig. 2c). Thus, also this new senescence marker classified 6-day-old *PaCypD* overexpressors as being senescent.

PaCypD overexpression and aging both lead to nuclear condensation

One of the most common apoptosis markers in mammalian cells is chromatin condensation and DNA fragmentation. Recently, morphological changes of nuclei have been found to occur also in fungi during apoptosis (Semighini *et al.*, 2006; Savoldi *et al.*, 2008). Consequently, we compared the nuclear morphology of juvenile (4 days old) and senescent (20 days old) wild-type cultures of *PaCypD* deletion strains and of 4-day-old *PaCypD* overexpressors. DAPI (4',6-Diamidino-2-phenylindole)-stained nuclei of juvenile wild-type and Δ*PaCypD* strains were round, while those of senescent hyphae from wild-type or Δ*PaCypD* show stretched and frayed contours. Within these structures, bright dense spots appear (Fig. 3, arrows). These changes in morphology are similar to those described as 'nuclear condensation' during apoptosis of the fungus *Aspergillus nidulans* (Semighini *et al.*, 2006; Savoldi *et al.*, 2008). Strikingly, DAPI-stained hyphae of the 4-day-old *PaCypD*_OEx revealed a senescent morphology of the nuclei, supporting the conclusion that, although chronologically young (4 days), *PaCypD* overexpressors show a senescent phenotype. Thus, 'nuclear condensation' appears to be a marker of senescence and of PCD in *P. anserina*.

Effects of cyclosporin A treatment

Human cyclophilins are known targets of CSA and are inhibited by this drug, a cyclic peptide that is used as an immunosuppressive in transplantation medicine and to treat Ullrich congenital muscular dystrophy, a degenerative human disease (Merlini *et al.*, 2008; Palma *et al.*, 2009). In our study, we addressed the

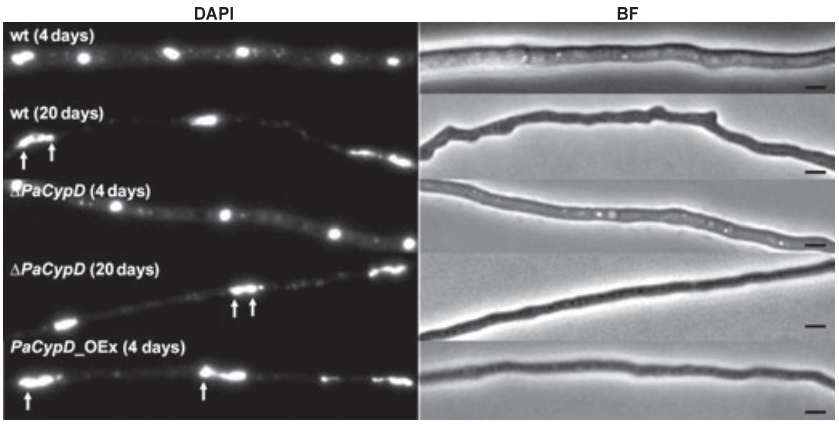

Fig. 3 Age- and PaCYPD-dependent changes of nuclear morphology. Representative hyphae (BF: bright field) and nuclei (DAPI: 4′,6-Diamidino-2-phenylindole) from wild-type strain 's', *PaCypD*_OEx and Δ*PaCypD* strains. Scale bars: 2 μm. Juvenile (4 days old) wild-type and Δ*PaCypD* strains display the characteristic spherical nuclei normally observed in healthy fungal cultures. Nuclei of senescent (20 days old) wild-type and Δ*PaCypD* strains are marked by deformations. These morphological changes are comparable to 'nuclear condensation' (arrows) described in apoptotic-like fungal cells. Hyphae of 4-day-old, prematurely aged *PaCypD* overexpressors already show nuclear condensation (arrows).

possibility that the putative *P. anserina* homolog PaCYPD is a target of CSA, as it is the case with CYPD from the closely related ascomycete *Neurospora crassa* (Tropschug *et al.*, 1989). In both, the wild-type and the *PaCypD* overexpression strain, the growth rate became affected when grown on CSA-containing medium. Addition of low concentrations of CSA resulted in a strong decrease in growth rate (Fig. 4a, b). Interestingly, the growth rates of the wild-type and of the analyzed *PaCypD* overexpressing strain, which differ on CSA-free medium, were found to be virtually identical on medium containing low amounts (0.02 and 0.04 μg mL^{-1}) of CSA, indicating that at these concentrations the drug restores growth of *PaCypD* overexpressors to wild-type growth. At higher concentrations (0.06 and 0.1 μg mL^{-1}), the growth rate of the wild-type remained almost stable but decreased drastically in the *PaCypD* overexpressing strain (Fig. 4b). Importantly, *PaCypD* deletion strains did not respond to the addition of CSA in the investigated concentration range. These observations suggest that a concentration-dependent specific inhibition of PaCYPD, but not of other cyclophilins, via the interaction with CSA is responsible for the observed effect on growth. Moreover, in accordance with earlier findings reported for *N. crassa* (Tropschug *et al.*, 1989; Bardiya & Shiu, 2007), the PaCYPD/CSA interaction product appears to inhibit the growth of *P. anserina* cultures. Therefore, at high CSA concentrations, the high abundance of PaCYPD in overexpressing strains results in a much stronger growth inhibition than in the wild-type strain.

Next, we investigated the impact of CSA on the lifespan of the different *P. anserina* strains (Table S5). Growth of the juvenile wild-type strain with low PaCYPD abundance (Fig. 4c) on medium containing 0.02 or 0.04 μg mL^{-1} CSA resulted in a 30% extension of the maximal lifespan. The mean lifespan increased only on medium containing 0.02 μg mL^{-1} CSA but not at higher concentrations. In the presence of 0.1 μg mL^{-1}, CSA neither mean nor maximum lifespan differ significantly from that on medium without CSA (Fig. 4c). At this high CSA concentration, it appears that the effect on lifespan after inhibition of PaCYPD is counteracted by the toxic CSA/PaCYPD interaction product.

As the abundance of PaCYPD increases during aging of *P. anserina* (Groebe *et al.*, 2007), we next investigated the effect of CSA in middle-aged wild-type stains that should contain slightly higher PaCYPD levels than juvenile strains. Middle-aged strains were obtained by growing juvenile cultures on standard medium (PASM) for 6 days before CSA was added. Concentrations of 0.02 and 0.04 μg mL^{-1} CSA had no positive effect on mean lifespan of these cultures (Fig. 4d). In contrast, compared to young cultures, 0.1 μg mL^{-1} CSA led to a clear lifespan extension supporting the expectation that these strains contain PaCYPD at a higher abundance than juvenile strains.

The effect on lifespan was finally investigated in *PaCypD* overexpressors. As described before, these strains have a drastically reduced lifespan, but growth on medium containing 0.02 or 0.04 μg mL^{-1} CSA increased the lifespan to that of the wild-type. In marked contrast, at elevated CSA concentrations (0.1 μg mL^{-1}), the level of the detrimental PaCYPD/CSA interaction product, which because of the abundance of PaCYPD is much higher in *PaCypD* overexpressors than in the wild-type, strongly shortens lifespan (Fig 4e). Most importantly, in the *PaCypD* deletion strain grown on medium with or without CSA, the lifespan is unaffected (Fig. 4f), suggesting that the effect of CSA on lifespan, as well as on growth rate, results from an interaction with PaCYPD and not with other cyclophilins.

Impairments of mitochondria in strains overexpressing *PaCypD*

Previous work reported the effect of reactive oxygen species (ROS) on the mPT (mitochondrial permeability transition) and on the mitochondrial membrane potential (Kroemer *et al.*, 2007). ROS are also known to increase in abundance during aging of *P. anserina* (Scheckhuber *et al.*, 2007). Consequently, we

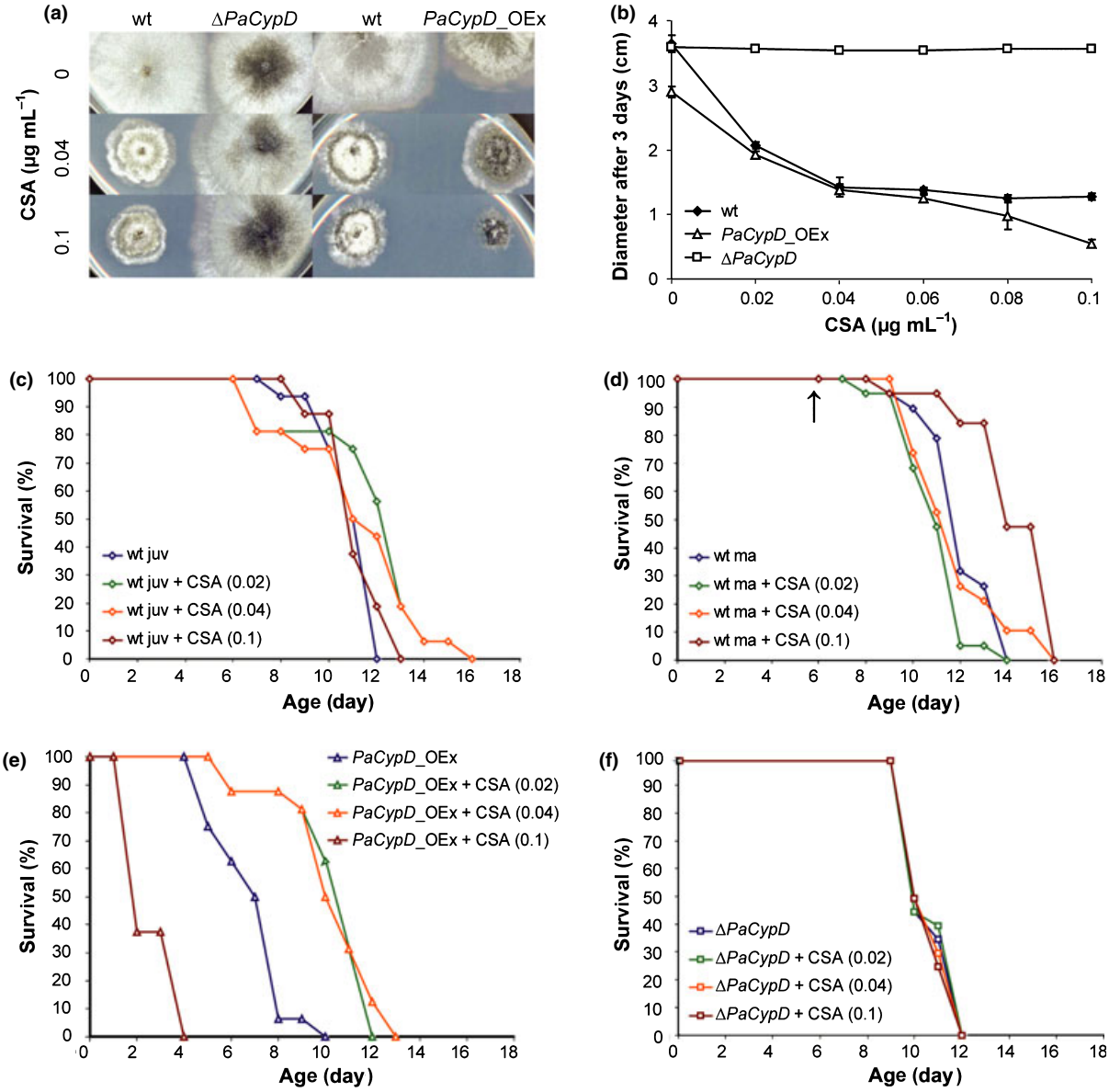

Fig. 4 Influence of cyclosporin A (CSA) on wild-type strain 's', Δ*PaCypD* and *PaCypD*_OEx. Statistical significance of all lifespan data (c–f) was demonstrated by the following tests: Wilcoxon (two-tailed), Log Rank (Mantel–Cox), Breslow (generalized Wilcoxon) and Tarone-Ware. (a) Colony morphology of wild-type strain 's', *PaCypD*_OEx and Δ*PaCypD* after 5 days growing on standard media with 0 μg mL^{-1}, 0.04 μg mL^{-1} and 0.1 μg mL^{-1} CSA. Growth of wild-type and *PaCypD*_OEx decreases, but adapts at 0.04 μg mL^{-1} CSA. At higher concentration, *PaCypD*_OEx is hardly able to grow. Δ*PaCypD* is not influenced by CSA. (b) Growth of wild-type strain 's' (n = 4), *PaCypD*_OEx (n = 4) and Δ*PaCypD* (n = 4) on standard media with 0 μg mL^{-1} (Δ: P = 7.7E-1; Ex: P = 2.8E-2), 0.02 μg mL^{-1} (Δ: P = 2.8E-2; Ex: P = 5.7E-1), 0.04 μg mL^{-1} (Δ: P = 2.8E-2; Ex: P = 8.3E-1), 0.06 μg mL^{-1}, 0.08 μg mL^{-1} and 0.1 μg mL^{-1} CSA (Δ: P = 2.8E-2; Ex: P = 2.8E-2). (c) Mean lifespan of wild-type strain 's' (n = 16) grown on standard media with 0 μg mL^{-1} (11.13 ± 1.15), 0.02 μg mL^{-1} (11.5 ± 3.41, P = 3E-2), 0.04 μg mL^{-1} (11 ± 3.39, P = 4.4E-1) and 0.1 μg mL^{-1} CSA (11.31 ± 1.2, P = 8.4E-1). Mean lifespan is significantly increased at 0.02 μg mL^{-1} CSA (for further statistical analyses see Table S3a). Also maximal lifespan is extended when wild-type cultures grow on 0.02 μg mL^{-1} and 0.04 μg mL^{-1} CSA. (d) Mean lifespan of wild-type strain 's' (n = 19) grown on 0 μg mL^{-1} (12.21 ± 1.4), 0.02 μg mL^{-1} (11.16 ± 1.3, P = 2.7E-2), 0.04 μg mL^{-1} (11.95 ± 1.9, P = 3.3E-1) and 0.1 μg mL^{-1} CSA (14.47 ± 1.9, P = 3.3E-4) after 6 days (arrow) of inoculation on standard media. Growth on 0.1 μg mL^{-1} CSA increases lifespan significantly (for further statistical analyses see Table S3b). (e) Mean lifespan of *PaCypD*_OEx (n = 16) grown on 0 μg mL^{-1} (7 ± 1.51), 0.02 μg mL^{-1} (10.38 ± 1.93, P = 1E-4), 0.04 μg mL^{-1} (10.38 ± 2.06, P = 1.2E-4) and 0.1 μg mL^{-1} CSA (2.75 ± 1, P = 1.55E-6). Lifespan of the *PaCypD* overexpressing strain increases upon addition of 0.02 μg mL^{-1} and 0.04 μg mL^{-1} CSA to the medium. 0.1 μg mL^{-1} CSA inhibits growth of *PaCypD*_OEx (for further statistical analyses see Table S3c). (f) Mean lifespan of Δ*PaCypD* (n = 20) grown on standard media with 0 μg mL^{-1} (11 ± 1), 0.02 μg mL^{-1} (10.85 ± 0.99, P = 9E-1), 0.04 μg mL^{-1} (10.8 ± 0.87, P = 9.6E-1) and 0.1 μg mL^{-1} CSA (10.75 ± 0.85, P = 9.5E-1). Δ*PaCypD* is not influenced by CSA. (for further statistical analyses, see Table S3d).

analyzed the mitochondrial membrane potential from different strains using the potential-dependent dye JC-1. Mitochondria treated with the uncoupler FCCP (carbonyl cyanide-p-triflouro-methoxy phenylhydrazone) and mitochondria heated to 100 °C served as controls. In comparison with wild-type mitochondria, those of the *PaCypD* overexpressor were characterized by a 21% reduction in membrane potential. In line with these data, potential-dependent Mitotracker Red uptake was impaired in

mitochondria of the *PaCypD* overexpressor. Moreover, in this strain only a few mitochondria were detectable in microscopic analyses. Strikingly, addition of CSA to mitochondrial samples of the transgenic strains restored the membrane potential to wild-type values (Fig. 5a).

As induction of mitochondria-triggered apoptosis is linked to the release of apoptogens from the intermembrane and intercristae space, we next investigated whether *PaCypD* overexpression leads to release of cytochrome *c* from mitochondria. Comparison of mitochondrial extracts from young wild-type cultures and *PaCypD* overexpressors (Fig. 5b) indicated a 66% reduction of cytochrome *c* abundance in mitochondria of the transgenic strain although transcript levels of cytochrome *c* were strongly increased (*PaCypD*_OEx1: 19.5-fold increase; *PaCypD*_OEx2: 11.6-fold increase) (Fig. 5c). It appears that increased transcript levels are the result of a compensatory mechanism to counteract cytochrome *c* loss from mitochondria. However, we were not able to detect cytochrome *c* in the cytoplasm of *PaCypD* overexpressing strains by Western blot analyses.

Mitochondria-associated stress and pro-apoptotic agents induce cell death via PaCYPD

The mitochondrial free radical theory of aging (Harman, 1972) suggests a central causative role of mitochondria in aging as the result of the generation of ROS during respiration and the age-related accumulation of ROS-induced molecular damage. ROS

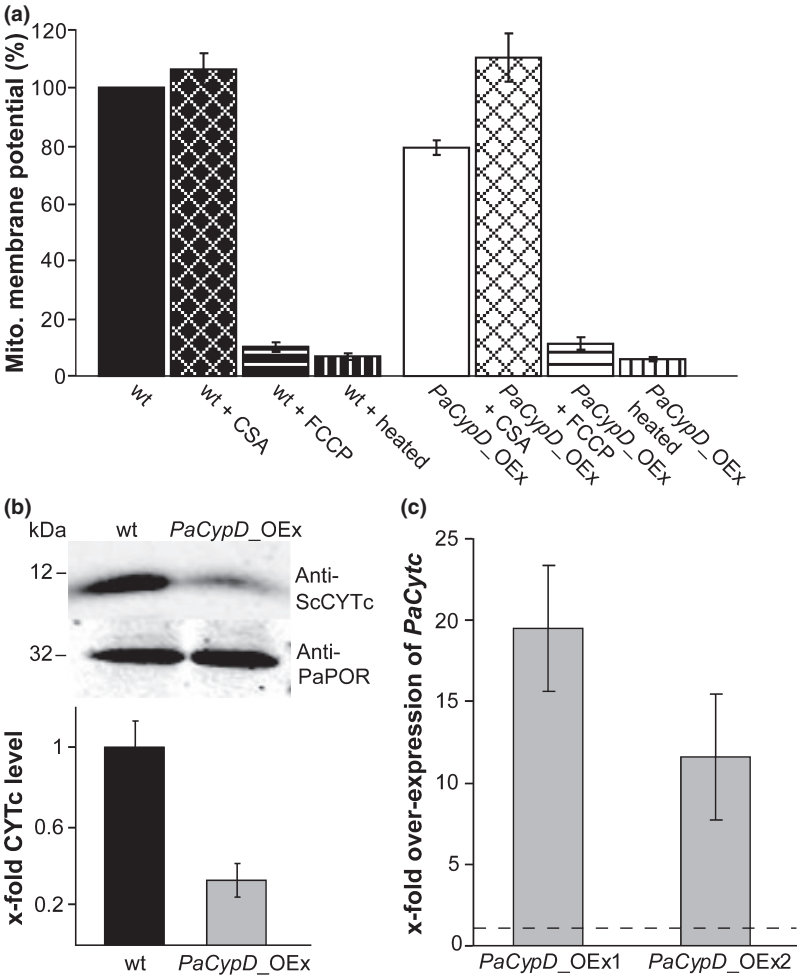

Fig. 5 Mitochondrial impairments of *PaCypD* overexpressing strains. (a) Mitochondrial membrane potential of juvenile (6 d) wild-type strain 's' (n = 4) and 6-day-old (presenescent) *PaCypD*_OEx strains (n = 4). Isolated mitochondria were either untreated (wt: 100; Ex: 79.14 ± 2.5, P = 2.8E-2), treated with 1 μM CSA (wt: 106.34 ± 5.42, P = 3.1E-1; Ex: 110.34 ± 8.33, P = 3.1E-1, P (Ex untreated) = 2.8E-2), or treated with 4 μM FCCP (control 1) and heated (control 2). *PaCypD*_OEx strains exhibit a lower mitochondrial membrane potential than wild-type strains. Treatment with CSA partially restores the mitochondrial membrane potential of *PaCypD*_OEx. (b) Protein level of cytochrome *c* visualized by Western blot analysis and by densitometry of mitochondrial protein extracts from juvenile (6 d) wild-type strain 's' (1 ± 0.13; n = 4) or presenescent (6 d) *PaCypD*_OEx (0.33 ± 0.08; n = 4, P = 2.8E-2). Predicted sizes of the proteins are shown on the left. PaPORIN was used as loading control for quantification. Cytochrome *c* level of mitochondria from *PaCypD* overexpressing strains is significantly reduced. (c) Transcription level of cytochrome *c* of juvenile (4 d) wild-type (1, n = 6, dashed line), 4- day-old *PaCypD*_OEx1 (19.5 ± 3.88, n = 6, P = 2.16E-3) and 4- day-old *PaCypD*_OEx2 (11.6 ± 3.84, n = 6, P = 2.16E-3) was determined by real-time PCR analysis. Expression was quantified relative to the *PaPorin* expression. *PaCytc* expression is increased in strains overexpressing *PaCypD*.

are also known to induce CYPD-dependent mPT and PCD (Kroemer *et al.*, 2007). Consequently, we investigated the different *P. anserina* strains used in this work for their ability to tolerate exogenous oxidative stress.

Addition of paraquat, an electron carrier that generates superoxide at the respiratory chain (Cocheme & Murphy, 2008), had a strong effect on growth rates. Growth of *PaCypD* overexpressors was most severely affected by paraquat. In contrast, in comparison with the wild-type, the tolerance of the deletion strain against this stressor was increased (Fig. 6a). Another inducer of oxidative stress with a role in aging and lifespan control is the micronutrient copper (Osiewacz & Borghouts, 2000; Stumpferl *et al.*, 2004; Scheckhuber *et al.*, 2009), an essential cofactor of different enzymes (e.g. cytochrome c oxidase, Cu/Zn superoxide dismutase). At higher concentrations, copper leads to the generation of the highly toxic hydroxyl radical by Fenton chemistry. Addition of this trace metal to the growth medium resulted in the strongest reduction in growth in the *PaCypD* overexpressors. In contrast, the deletion strain shows a slight but significant increase in copper tolerance (Fig. 6b).

Next, we investigated the effect of specific inducers of fungal apoptosis on the growth rate of the wild-type, *PaCypD*_OEx and Δ*PaCypD* strains. The lipid phytosphingosine is known to induce apoptosis in the filamentous fungi *Aspergillus nidulans* and *Neurospora crassa* (Cheng *et al.*, 2003; Castro *et al.*, 2008). Compared to the wild-type, growth of the *PaCypD* overexpressing strains on medium containing phytosphingosine was strongly reduced. In contrast, *PaCypD* deletion strains show a high resistance against this drug (Fig. 6c). Consistently, addition of farnesol, another drug triggering PCD in *A. nidulans* (Semighini *et al.*, 2006), identified *PaCypD* overexpressors as being more sensitive to the drug than the wild-type. *PaCypD* deletion strains are characterized by the highest tolerance to farnesol (Fig. 6d).

Discussion

In this study, we establish a novel mechanistic link between PCD and organismal aging triggered by a mitochondrial pathway, in which cyclophilin D plays a central role. This link is supported by the earlier observation of an increase in PaCYPD abundance during aging of *P. anserina* (Groebe *et al.*, 2007), by genetic manipulation of PaCYPD abundance and by inhibition of PaCYPD *via* the cyclic peptide CSA. Based on our data and referring to a general model of mPTP formation and regulation (Schneider, 2005; Kroemer *et al.*, 2007), we propose a mechanism that is effective at the end of the life cycle of

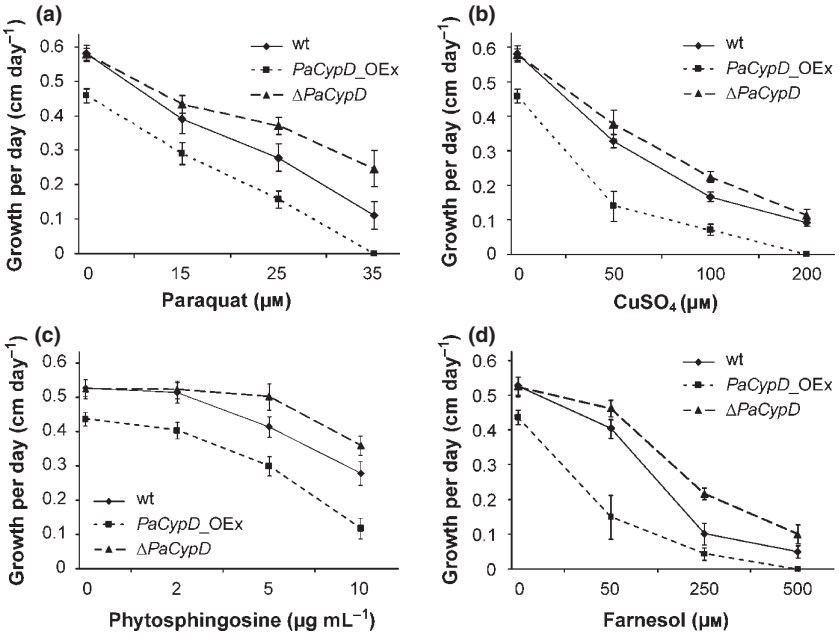

Fig. 6 Stress response of wild-type strain 's', Δ*PaCypD* and *PaCypD*_OEx. (a) Growth rate of wild-type strain 's' (n = 16), *PaCypD*_OEx (n = 16) and Δ*PaCypD* (n = 16) on standard media with 0 μM (Δ: P = 6.6E-1; Ex: P = 1.55E-6), 15 μM (Δ: P = 1.04E-3; Ex: P = 1.89E-5), 25 μM (Δ: P = 2.25E-6; Ex: P = 1.55E-6) and 35 μM paraquat (Δ: P = 6.11E-6; Ex: P = 1.55E-6). Treatment with paraquat resulted in a decreased growth rate of the *PaCypD* overexpressing strain, while paraquat resistance of Δ*PaCypD* is strongly increased. (b) Growth rate of wild-type strain 's' (n = 16), *PaCypD*_OEx (n = 16) and Δ*PaCypD* (n = 16) on standard medium with 0 μM (Δ: P = 6.6E-1; Ex: P = 1.55E-6), 50 μM (Δ: P = 1.45E-3; Ex: P = 1.55E-6), 100 μM (Δ: P = 2.7E-6; Ex: P = 1.55E-6) and 200 μM $CuSO_4$ (Δ: P = 7.96E-4; Ex: P = 1.55E-6). Treatment with low levels of copper resulted in a dramatic growth rate decrease in the *PaCypD* overexpressing strain, while copper resistance of Δ*PaCypD* is increased. (c) Growth rate of wild-type strain 's' (n = 16), *PaCypD*_OEx (n = 16) and Δ*PaCypD* (n = 16) on standard media with 0 μg mL^{-1} (Δ: P = 7.8E-1; Ex: P = 3.3E-9), 2 μg mL^{-1} (Δ: P = 4.9E-1; Ex: P = 3.3E-9), 5 μg mL^{-1} (Δ: P = 2.2E-7; Ex: P = 3.3E-9) and 10 μg mL^{-1} phytosphingosine (Δ: P = 2.3E-8; Ex: P = 3.3E-9). Treatment with phytosphingosine resulted in a decreased growth rate of the *PaCypD* overexpressing strain, while phytosphingosine resistance of Δ*PaCypD* is strongly increased. (d) Growth rate of wild-type strain 's' (n = 16), *PaCypD*_OEx (n = 16) and Δ*PaCypD* (n = 16) on standard media with 0 μM (Δ: P = 7.8E-1; Ex: P = 3.3E-9), 50 μM (Δ: P = 6.9E-6; Ex: P = 3.3E-9), 250 μM (Δ: P = 3.3E-9; Ex: P = 1.5E-7) and 500 μM farnesol (Δ: P = 4.6E-7; Ex: P = 3.3E-9). Already, treatment with low farnesol concentrations resulted in a severe growth rate decrease in the *PaCypD* overexpressing strain, while farnesol resistance of Δ*PaCypD* is significantly increased.

P. anserina. We suggest that in senescent strains, PaCYPD interacts with a component of the mPTP in the inner mitochondrial membrane, most likely the adenine nucleotide translocator ANT, resulting in the opening of the pore. As a consequence, water and solutes up to 1.5 kDa cross both mitochondrial membranes resulting in mitochondrial swelling, in breakdown of the membrane potential, rupture of the outer mitochondrial membrane and consequently the release of pro-apoptotic factors from the inner membrane and the intercristae space (Schneider, 2005; Kroemer *et al.*, 2007). Although the structure and regulation of this mitochondrial membrane complex are not finally solved, and notwithstanding the ongoing controversial discussion (Vieira *et al.*, 2000; Leung & Halestrap, 2008; Leung *et al.*, 2008), it is widely accepted that the mitochondrial peptidyl prolyl-*cis,trans*-isomerase CYPD plays a key role in opening the mPTP (Halestrap, 2009). Other key components in the process are ROS that trigger mPTP opening. These compounds are well known to accumulate during aging of *P. anserina* (Scheckhuber *et al.*, 2007). Together with the increase in PaCYPD abundance, ROS are likely to trigger mPTP opening in the final stage of the *P. anserina* life cycle. In this study, this role of ROS is strongly supported by our finding that strains overexpressing *PaCypD* are more sensitive against exogenous mitochondrial stressors like paraquat and copper. In contrast, the *PaCypD* deletion strain shows increased tolerance against these stressors. A similar protection against oxidative stress-induced cell death was previously reported for primary hepatocytes and fibroblasts from CYPD-deficient mice (Baines *et al.*, 2005), suggesting a role of oxidative stress in the induction of CYPD-mediated cell death. In addition, we found that pro-apoptotic agents like phytosphingosine and farnesol appear to induce PCD in *P. anserina*. This process is PaCYPD dependent as demonstrated by the strongly reduced growth rate of *PaCypD* overexpressors and a significantly increased resistance of the *PaCypD* deletion strains against these apoptosis inducers. Interestingly, Castro *et al.* (2008) found that *N. crassa* mutants, which are more resistant against ROS than wild-type strains, also display a high phytosphingosine resistance. These results, similar to our observations in the *PaCypD* deletion strains, connect ROS with the induction of PCD and identify PaCYPD as an important factor triggering ROS-, sphingolipid- and farnesol-induced PCD in the aging model *P. anserina*.

Key results supporting our conclusions are derived from the experiments using CSA as a cyclophilin inhibitor. There are a number of different putative cyclophilins encoded in the genome of *P. anserina,* which may all be inhibited by CSA. However, in our experiments, it is the specific interaction of CSA with PaCYPD, which is responsible for the observed changes in growth rate and lifespan. This is clearly demonstrated by the characteristics of the *PaCypD* deletion strain. Within the investigated concentration range of the drug, this strain does not show any change in neither growth rate nor lifespan. On first glance, the latter may be surprising given the observation that overexpression of *PaCypD* leads to accelerated aging because of the induction of PCD. However, this can be explained by the fact that multiple, redundant pathways are effective in controlling a mechanism that has such serious consequences as PCD. After deletion of one of these pathways, other pathways may become effective. Experimental data obtained for *CypD*-independent cell death in mice are in accordance with this conclusion. It has previously been reported from mice that in cells lacking CYPD, several pro-apoptotic agents like staurosporine and etoposide induce cell death at a similar rate as in wild-type cells (Nakagawa *et al.*, 2005). In addition, normal mPTP opening was found to occur in response to arsenicals (Basso *et al.*, 2005) in mouse mitochondria lacking CYPD, indicating that CYPD-independent mPTP opening is possible. Alternatively, or in addition to PaCYPD-independent mechanisms limiting lifespan, the expected lifespan increase in the *PaCypD* deletion strain may be counteracted by a lack of vital PaCYPD functions, e.g. a chaperone-like function described for the yeast PaCYPD homolog named CPR3. This mitochondrial peptidyl prolyl-*cis, trans*-isomerase has been demonstrated to accelerate the refolding of a fusion protein imported into the matrix of isolated yeast mitochondria (Matouschek *et al.*, 1995).

The demonstration of early expression of markers of senescence, like mtDNA instabilities, impairments in fertility, increased transcript levels of the metallothionein gene (*PaMt1*) and loss of superoxide dismutase 2 (PaSOD2) activity, changes in mitochondrial network and ultrastructure in *PaCypD* overexpressors clearly disclose that the shortening in lifespan in these strains results from the acceleration of genuine aging processes. A decrease in mitochondrial cytochrome *c* levels and membrane potential links these processes to PCD (Ly *et al.*, 2003). Failure to demonstrate an increase in cytosolic cytochrome *c* in *PaCypD* overexpressors, which are known to have lower levels of mitochondrial cytochrome *c,* is well in accordance with experimental data from L929sAhFas cells, a murine fibrosarcoma cell line, during anti-Fas-induced cell death (Denecker *et al.*, 2001). Another new link between fungal senescence and PCD was detected by microscopy. Senescent hyphae display changes of nuclear morphology comparable to the apoptosis-dependent 'nuclear condensation' described previously in other filamentous fungi (Semighini *et al.*, 2006; Savoldi *et al.*, 2008). Remarkably, nuclei of 4-day-old *PaCypD*_OEx cultures are characterized by the nuclear morphology characteristic for senescent *P. anserina* cultures. These results are in accordance with the conclusion that *PaCypD* overexpressors are functionally senescent and have induced the PCD machinery at the chronologically young age of 4 days. Moreover, it appears that the nuclear morphology in *P. anserina* is a marker for both senescence and PCD.

The challenge is now to identify other components involved in mitochondrial pore formation and to elucidate their function in PCD during aging. It has recently been demonstrated that CYPD binding to F_0F_1ATPase from bovine heart mitochondria decreases its activity and points to an intriguing possibility of PaCYPD as a modulator of mitochondrial ATP synthesis (Giorgio *et al.*, 2009). Such a potential regulatory function of PaCYPD may also be linked to PCD induction and death of

P. anserina cultures and thus presents one specific perspective for future studies. Moreover, it will be interesting to see whether or not the mechanisms reported in this study are conserved among organisms. The recent report of an age-related increase in CYPD in rat gastrocnemius muscle and in brain tissue of mice and humans (Du *et al.*, 2008; Marzetti *et al.*, 2008) as well as the age-related loss of muscle mass (sarcopenia) leading to frailty in humans makes it likely that PCD plays an important role also in human aging and in age-related degeneration at least of certain tissues such as brain and muscle. There already is widespread experience in administering CSA, a cyclic peptide approved for human therapy in transplantation medicine or for treatment of Ullrich congenital muscular dystrophy, the human degenerative disorder. This drug has recently also been suggested for Alzheimer therapy, because CYPD was found to interact with the mitochondrial amyloid-ß protein and increases neuronal and synaptic stress (Du *et al.*, 2008). Another immunosuppressive drug, rapamycin, which is mainly used in transplantation medicine in combination with CSA (Kahan, 2008), has recently been demonstrated to decelerate cellular senescence (Demidenko *et al.*, 2009). Feeding rapamycin to middle-aged mice was found to increase their lifespan by 9-18% (Harrison *et al.*, 2009). This agrees well with the 18.5% extension of mean lifespan of middle-aged *P. anserina* wild-type strains treated with CSA. Our finding that the dramatically reduced lifespan of strains overexpressing *PaCypD* is reverted to the wild-type-specific lifespan by CSA is in line with these observations.

Experimental procedures

Strains and culture conditions

The wild-type 's' (Rizet, 1953) strain of *P. anserina* was used. The deletion strain Δ*PaCypD* and the overexpression strains *PaCypD*_OEx1 and *PaCypD*_OEx2 were generated in the genetic background of this wild-type strain. All strains were grown on *P. anserina* synthetic medium (PASM) with 1% glucose (Hamann *et al.*, 2007) at 27 °C under constant light. To obtain cultures of a defined age, mycelium from freshly germinated spores was placed on one side of a Petri dish containing 30 mL of PASM. Every 2–3 days, the growth front was marked. After reaching the other side of the Petri dish, fresh plates of PASM were inoculated with a piece of the culture obtained from the growth front. For further analysis, senescent cultures were obtained from plates shortly before growth arrest to inoculate fresh plates (e.g. isolation of senescent mitochondria).

Lifespan and growth rate

Lifespan and growth rate were determined for monokaryotic isolates from independent crosses, placed on one side of a Petri dish containing 30 mL of PASM. To analyze growth on CSA, PASM plates were supplemented with 0.02, 0.04 and 0.1 μg mL^{-1} CSA, respectively, and incubated in the dark. Growth was measured until it stopped. The period of linear growth was recorded as lifespan in days. During this period, the growth rate was measured in centimeters per day. Mean lifespan was determined as the average of all lifespans from monokaryotic isolates of one strain.

Fertility analysis

To assess fertility, mycelia from wild-type strain 's', *PaCypD*_OEx or Δ*PaCypD* of both mating types were allowed to overgrow the surface of plates containing corn meal extract (BMM) complete medium (Esser, 1974) at 27 °C under constant light. Spermatia of the male partner were harvested by flooding the plates with 5 mL of sterile water. From this suspension, 300 μL were pipetted onto mycelia of the female partner of the opposite mating type. After 5 min, the drops were removed carefully. Fourteen to 24 days after fertilization, the number of perithecia was counted. The resulting values were divided by the area of the drop. The number of perithecia developing on plates overgrown with wild-type 's' and fertilized with wild-type spermatia was set to 100% fertility.

Growth on copper sulfate, paraquat, farnesol, phytosphingosine and CSA

Growth on $CuSO_4$, paraquat, farnesol, phytosphingosine and CSA, respectively, was determined after 3 days using monokaryotic isolates from wild-type strain 's', *PaCypD*_OEx or Δ*PaCypD* strains inoculated on PASM plates containing different amounts of each substance. Plates with CSA, farnesol and phytosphingosine were incubated in the dark. Except for the growth on CSA, growth rates were calculated as growth per day (cm/d).

Construction of deletion strain Δ*PaCypD*

Deletion of *PaCypD* in wild-type strain 's' (mating type) was performed according to a previously described method (Hamann *et al.*, 2005). Briefly, small flanking regions of *PaCypD* were amplified using the 5′-flank oligonucleotides KOCyclo1 (5′-TTGGTACCCGTCTCAACTCTTCCTCC-3′) and KOCyclo2 (5′-GGAAGCTTGGTTAGTGCTCCACATGG-3′), introducing *Kpn*I and *Hin*dIII restriction sites and the 3′-flank oligonucleotides KOCyclo3 (5′-GGGGACTAGTTCGGAACGAAGGAGGGTG-3′), and KOCyclo4 (5′- TTGCGGCCGCCGGAAGAGCGCGACTTTG-3′) introducing *Bcu*I and *Not*I restriction sites. The fragments were cloned into pKO4 5′ and 3′ next to the bifunctional resistance cassette consisting of a blasticidin resistance gene (*bsd*) for selection in *E. coli* and a phleomycin resistance gene (*ble*) for selection in *P. anserina*. The resistance cassette with the flanking regions was excised by restriction with *Not*I and *Kpn*I and used to transform *E. coli* strain KS272 bearing the plasmid pKOBEG (Chaveroche *et al.*, 2000) and a cosmid isolated from a cosmid library of *P. anserina* wild-type strain 's' (Osiewacz, 1994) containing the *PaCypD* locus. Homologous recombination between the flanks of the resistance cassette and the cosmid produced a

deletion cosmid, which was isolated and used to transform *P. anserina* spheroplasts. Transformants were selected by growth on phleomycin-containing medium. The cosmid also bears a hygromycin B (*hph*) resistance cassette. Transformants carrying the correct replacement after homologous recombination (Δ*PaCypD*) are ble resistant and hph sensitive.

Construction of overexpressing strains *PaCypD*_OEx1 and *PaCypD*_OEx2

The open reading frame including a ~500 bp terminator region encoding for *PaCypD* was amplified by PCR with Phusion polymerase (Finnzymes, Espoo, Finland) using the oligonucleotides CycloExfor (5′- CCGGATCCATGTTTCGACCCCTCCTA-3′) and CycloExrev (5′- GGCTGCAGGGGGGGATATCGTGTTAGG-3′) introducing *Bam*HI and *Pst*I restriction sites. The generated PCR product was digested with *Bam*HI and *Pst*I and cloned into the expression vector pExMthph behind the 0.5 kb promoter fragment of the metallothionein gene (*PaMt1*) (Averbeck *et al.*, 2001). The nucleotide sequence of the constructed overexpression vector was verified by sequencing (SRD GmbH, Oberursel, Germany) and transformed into wild-type spheroplasts. Transformants were selected by growth on hph-containing medium, as pExMthph contains a hygromycin B (*hph*) resistance cassette.

Southern blot analysis

Total DNA was isolated according to Lecellier and Silar (1994). DNA restriction, gel electrophoresis and Southern blotting were performed according to standard protocols. Digoxigenin-labeled gene probes covering part of the open reading frame of *PaCypD* or of the blasticidin gene (part of the bifunctional resistance cassette, *bsd*) were used to identify *PaCypD* overexpressing and deletion strains. MtDNA rearrangements were determined with a digoxigenin-labeled plDNA probe generated from plasmid pSP17 (Borghouts *et al.*, 1997). The *grisea* probe was used as a loading control. For Southern blot hybridization and detection, the instructions of the manufacturer (Roche, Germany) were followed.

Transcript analysis

Plates containing PASM covered with a layer of cellophane were inoculated with small pieces of mycelium from freshly germinated spores and incubated for 3 days at 27 °C under constant light. Total RNA was isolated from scraped fungal mycelium of the inoculated PASM plates using the RNeasy Plant Mini Kit (Qiagen). cDNA synthesis was performed with the iScript cDNA Synthesis Kit (BioRad) according to the manufacturers' instruction. For RT-PCR experiments, *Taq* DNA Polymerase (Invitrogen) was used, real-time PCR was realized by iQ SYBR Green Supermix (BioRad) followed by the manufacturers' protocol. Table S1 lists oligonucleotides used for RT-PCR and/or real-time PCR. The real-time PCR experiments were performed using the MiniOpticon (BioRad). The efficiency (E) of the primer pairs was calculated based on a real-time PCR with a dilution series of cDNA according to $E = 10^{[-1/Slope]}$. Using the efficiency and the crossing point deviation, it was possible to determine the expression ratio (R) (Pfaffl, 2001) relative to the *PaPorin* expression.

Isolation of mitochondria

Mitochondria of *P. anserina* cultures were isolated by differential centrifugation and purified using a 20–50% discontinuous sucrose gradient as described previously (Kunstmann & Osiewacz, 2008).

SDS-PAGE and Western blot analysis

Fifty micrograms of mitochondrial protein samples were incubated at 95 °C for 10 min in loading buffer [0.1 M Tris (ph 6.8), 6% SDS, 6% glycerol, 0.6 M ß-mercaptoethanol] and were separated on a 16% SDS-PAGE. Subsequently, separated proteins were transferred to a PVDF membrane (Immobilon-FL, Millipore, Schwalbach, Germany) using an electro-blotter (Bio-Rad). Western blots were probed with a polyclonal *P. anserina* cyclophilin D antibody (Anti-PaCYPD) (1:5000, overnight, 4 °C), a *S. cerevisiae* cytochrome *c* antibody (Anti-ScCYTc) (1:5000, overnight, 4 °C) or a monoclonal HSP60 (mouse) antibody (Anti-HSP60) (1:4000, overnight, 4 °C) from Biomol Stressgen (#SPA-807). The loading of mitochondria was confirmed by incubation with a polyclonal antibody against PaPORIN (Anti-PaPOR) (1:5000, overnight, 4 °C). Labeling was detected with IRDye 800–conjugated goat-anti-rabbit antibody (1:10 000, 1 h, RT) and scanning the blots with an Odyssey infrared scanner (Li-Cor, Lincoln, NE, USA), using the Odyssey analysis software for quantification.

SOD activity measurements

Total protein was extracted as described previously (Kunstmann & Osiewacz, 2008). Hundred micrograms of total protein were separated on a native 8.5% polyacrylamide gel and stained using nitroblue tetrazolium (NBT), riboflavin and *N*,*N*,*N*′,*N*′-tetramethylethylenediamine (Borghouts *et al.*, 2001). Gels were developed on a light box and scanned.

Mitochondrial membrane potential measurements

Mitochondria of *P. anserina* cultures were isolated by differential centrifugation and diluted in incubation buffer as previously described (Gredilla *et al.*, 2006). Inhibitors (1 μM CSA; 4 μM FCCP) were added to 300 μg mitochondria and incubated for 10 min at 27 °C. Samples of untreated or heated (10 min, 100 °C) mitochondria were incubated identically. After addition of substrates (20 mM pyruvate/5 mM malate) and incubation for 1 min at 27 °C, samples were mixed with 0.2 μg mL^{-1} JC-1 followed by an incubation step for 10 min at 27 °C. 300 μM ADP were added, samples were incubated for 1 min at 27 °C and portioned into three wells of a black 96-well plate. The

fluorescence intensity was recorded at 536 and 595 nm (emission) after excitation at 490 nm in a multiplate reader (Saphire 2, TECAN) at 27 °C. Green JC-1 monomers, mainly in collapsed mitochondria, can be detected at 536 nm; red JC-1 aggregates, accumulating in mitochondria with intact membrane potential, are detectable at 595 nm. Ratio of 595/536 nm was determined and wild-type value was set to 100%.

Fluorescence microscopy

For fluorescence microscopy, slide cultures (Riddell, 1950) of wild-type 's', *PaCypD*_OEx or Δ*PaCypD* were prepared and treated with Mitotracker Red CMXRos (Invitrogen) or with the DNA dye DAPI. Hyphae were visualized using a fluorescence microscope (DM LB, Leica, Wetzlar, Germany) equipped with the appropriate excitation and emission filters. A digital camera system (Canon, Tokyo, Japan) connected to the microscope was used for documentation.

Electron cryo-tomography

Mitochondria of *P. anserina* isolated by differential centrifugation (Gredilla *et al.*, 2006) were diluted with isolation buffer and mixed 1:1 with a 6 nm colloidal gold solution as fiducial markers. The final concentration of the suspension was 2.5 mg mL^{-1}. Three microliters of the solution was applied to a glow discharged Quantifoil specimen support grid, blotted for 5 s from one side in a humidified atmosphere and immediately plunge frozen in liquid ethane.

Grids were mounted under liquid nitrogen and transferred at a temperature of 95 K into an FEI Polara electron microscope equipped with a field emission gun operated at 300 kV. Images were recorded with a 2 × 2k 863 GIF Tridiem energy filter (Gatan, Pleasanton, CA, USA) at 6–8 μm underfocus at a specimen temperature of 82 K, using a slit width of 20 eV. Uniaxial tilt series were recorded from +65 ° to −65 ° at intervals of 1.5 °, with a total dose of 1–1.5 × 10^4 e nm^{-2}. Volume reconstruction was performed using the IMOD tomography software (Kremer *et al.*, 1996) and subjected to 10 intervals of denoising by nonlinear anisotropic diffusion (Frangakis & Hegerl, 2001). Segmentation and analysis of the tomographic volumes was carried out manually with AMIRA (Mercury Systems, Düsseldorf, Germany).

Sequence analysis

The alignment of cyclophilin D homologs from different organisms was performed using the CLUSTALW2 sequence alignment software (Larkin *et al.*, 2007). The putative mitochondrial localization sequence was obtained from the MitoProt data base (Claros & Vincens, 1996).

Statistical analysis

Comparisons between different samples were statistically analyzed with Wilcoxon test, two-tailed. The minimum level of statistical significance was set at $P < 5.0E\text{-}2$ for all analyses. The mean value ± SD is shown. To ensure the significant lifespan changes received by Wilcoxon test, two-tailed, three additional statistical tests were performed using the SPSS statistics software: Log Rank (Mantel–Cox), Breslow (generalized Wilcoxon) and Tarone-Ware.

Acknowledgments

The research was supported by grants of the Deutsche Forschungsgemeinschaft (Os75/12-1) and by the European Commission via the Integrated Project with the acronym *MiMage*; (LSHM-CT-2004-512020). We thank Prof. R. Lill (Phillips University Marburg, Germany) for providing the antibody against cytochrome *c*.

References

Averbeck NB, Borghouts C, Hamann A, Specke V, Osiewacz HD (2001) Molecular control of copper homeostasis in filamentous fungi: increased expression of a metallothionein gene during aging of *Podospora anserina*. *Mol. Gen. Genet.* **264**, 604–612.

Baines CP (2009) The molecular composition of the mitochondrial permeability transition pore. *J. Mol. Cell. Cardiol.* **46**, 850–857.

Baines CP, Kaiser RA, Purcell NH, Blair NS, Osinska H, Hambleton MA, Brunskill EW, Sayen MR, Gottlieb RA, Dorn GW, Robbins J, Molkentin JD (2005) Loss of cyclophilin D reveals a critical role for mitochondrial permeability transition in cell death. *Nature* **434**, 658–662.

Bardiya N, Shiu PK (2007) Cyclosporin A-resistance based gene placement system for *Neurospora crassa*. *Fungal Genet. Biol.* **44**, 307–314.

Basso E, Fante L, Fowlkes J, Petronilli V, Forte MA, Bernardi P (2005) Properties of the permeability transition pore in mitochondria devoid of Cyclophilin D. *J. Biol. Chem.* **280**, 18558–18561.

Borghouts C, Kimpel E, Osiewacz HD (1997) Mitochondrial DNA rearrangements of *Podospora anserina* are under the control of the nuclear gene *grisea*. *Proc. Natl. Acad. Sci. U S A* **94**, 10768–10773.

Borghouts C, Werner A, Elthon T, Osiewacz HD (2001) Copper-modulated gene expression and senescence in the filamentous fungus *Podospora anserina*. *Mol. Cell. Biol.* **21**, 390–399.

Borghouts C, Scheckhuber CQ, Werner A, Osiewacz HD (2002) Respiration, copper availability and SOD activity in *P. anserina* strains with different lifespan. *Biogerontology* **3**, 143–153.

Brust D, Hamann A, Osiewacz HD (2009) Deletion of *PaAif2* and *PaAmid2*, two genes encoding mitochondrial AIF-like oxidoreductases of *Podospora anserina*, leads to increased stress tolerance and lifespan extension. *Curr. Genet.* **55**, 225–235.

Castro A, Lemos C, Falcão A, Glass NL, Videira A (2008) Increased resistance of complex I mutants to phytosphingosine-induced programmed cell death. *J. Biol. Chem.* **283**, 19314–19321.

Chaveroche MK, Ghigo JM, d'Enfert C (2000) A rapid method for efficient gene replacement in the filamentous fungus *Aspergillus nidulans*. *Nucleic Acids Res.* **28**, E97.

Cheng J, Park TS, Chio LC, Fischl AS, Ye XS (2003) Induction of apoptosis by sphingoid long-chain bases in *Aspergillus nidulans*. *Mol. Cell. Biol.* **23**, 163–177.

Claros MG, Vincens P (1996) Computational method to predict mitochondrially imported proteins and their targeting sequences. *Eur. J. Biochem.* **241**, 779–786.

Cocheme HM, Murphy MP (2008) Complex I is the major site of mitochondrial superoxide production by paraquat. *J. Biol. Chem.* **283**, 1786–1798.

Demidenko ZN, Zubova SG, Bukreeva EI, Pospelov VA, Pospelova TV, Blagosklonny MV (2009) Rapamycin decelerates cellular senescence. *Cell Cycle* **8**, 1888–1895.

Denecker G, Vercammen D, Steemans M, Vanden BT, Brouckaert G, van LG, Zhivotovsky B, Fiers W, Grooten J, Declercq W, Vandenabeele P (2001) Death receptor-induced apoptotic and necrotic cell death: differential role of caspases and mitochondria. *Cell Death Differ.* **8**, 829–840.

Du H, Guo L, Fang F, Chen D, Sosunov AA, McKhann GM, Yan Y, Wang C, Zhang H, Molkentin JD, Gunn-Moore FJ, Vonsattel JP, Arancio O, Chen JX, Yan SD (2008) Cyclophilin D deficiency attenuates mitochondrial and neuronal perturbation and ameliorates learning and memory in Alzheimer's disease. *Nat. Med.* **14**, 1097–1105.

Esser K (1974) *Podospora anserina*. *in Handbook of Genetics* (King RC, ed). New York: Plenum Press, pp. 531–551.

Fadeel B, Orrenius S (2005) Apoptosis: a basic biological phenomenon with wide-ranging implications in human disease. *J. Intern. Med.* **258**, 479–517.

Frangakis AS, Hegerl R (2001) Noise reduction in electron tomographic reconstructions using nonlinear anisotropic diffusion. *J. Struct. Biol.* **135**, 239–250.

Giorgio V, Bisetto E, Soriano ME, Dabbeni-Sala F, Basso E, Petronilli V, Forte MA, Bernardi P, Lippe G (2009) Cyclophilin D modulates mitochondrial F_0F_1-ATP synthase by interacting with the lateral stalk of the complex. *J. Biol. Chem.* **284**, 33982–33988.

Golstein P, Kroemer G (2007) Cell death by necrosis: towards a molecular definition. *Trends Biochem. Sci.* **32**, 37–43.

Gredilla R, Grief J, Osiewacz HD (2006) Mitochondrial free radical generation and lifespan control in the fungal aging model *Podospora anserina*. *Exp. Gerontol.* **41**, 439–447.

Grimm S, Brdiczka D (2007) The permeability transition pore in cell death. *Apoptosis* **12**, 841–855.

Groebe K, Krause F, Kunstmann B, Unterluggauer H, Reifschneider NH, Scheckhuber CQ, Sastri C, Stegmann W, Wozny W, Schwall GP, Poznanovic S, Dencher NA, Jansen-Dürr P, Osiewacz HD, Schrattenholz A (2007) Differential proteomic profiling of mitochondria from *Podospora anserina*, rat and human reveals distinct patterns of age-related oxidative changes. *Exp. Gerontol.* **42**, 887–898.

Halestrap AP (2009) What is the mitochondrial permeability transition pore? *J. Mol. Cell. Cardiol.* **46**, 821–831.

Hamann A, Krause K, Werner A, Osiewacz HD (2005) A two-step protocol for efficient deletion of genes in the filamentous ascomycete *Podospora anserina*. *Curr. Genet.* **48**, 270–275.

Hamann A, Brust D, Osiewacz HD (2007) Deletion of putative apoptosis factors leads to lifespan extension in the fungal ageing model *Podospora anserina*. *Mol. Microbiol.* **65**, 948–958.

Hamann A, Brust D, Osiewacz HD (2008) Apoptosis pathways in fungal growth, development and ageing. *Trends Microbiol.* **16**, 276–283.

Harman D (1972) The biologic clock: the mitochondria? *J. Am. Geriatr. Soc.* **20**, 145–147.

Harrison DE, Strong R, Sharp ZD, Nelson JF, Astle CM, Flurkey K, Nadon NL, Wilkinson JE, Frenkel K, Carter CS, Pahor M, Javors MA, Fernandez E, Miller RA (2009) Rapamycin fed late in life extends lifespan in genetically heterogeneous mice. *Nature* **460**, 392–395.

Kahan BD (2008) Fifteen years of clinical studies and clinical practice in renal transplantation: reviewing outcomes with de novo use of sirolimus in combination with cyclosporine. *Transplant. Proc.* **40**, S17–S20.

Kremer JR, Mastronarde DN, McIntosh JR (1996) Computer visualization of three-dimensional image data using IMOD. *J. Struct. Biol.* **116**, 71–76.

Kroemer G, Galluzzi L, Brenner C (2007) Mitochondrial membrane permeabilization in cell death. *Physiol. Rev.* **87**, 99–163.

Kunstmann B, Osiewacz HD (2008) Over-expression of an S-adenosylmethionine-dependent methyltransferase leads to an extended lifespan of *Podospora anserina* without impairments in vital functions. *Aging Cell* **7**, 651–662.

Larkin MA, Blackshields G, Brown NP, Chenna R, McGettigan PA, McWilliam H, Valentin F, Wallace IM, Wilm A, Lopez R, Thompson JD, Gibson TJ, Higgins DG (2007) Clustal W and Clustal X version 2.0. *Bioinformatics* **23**, 2947–2948.

Lecellier G, Silar P (1994) Rapid methods for nucleic acids extraction from Petri dish-grown mycelia. *Curr. Genet.* **25**, 122–123.

Leung AW, Halestrap AP (2008) Recent progress in elucidating the molecular mechanism of the mitochondrial permeability transition pore. *Biochim. Biophys. Acta* **1777**, 946–952.

Leung AW, Varanyuwatana P, Halestrap AP (2008) The mitochondrial phosphate carrier interacts with cyclophilin D and may play a key role in the permeability transition. *J. Biol. Chem.* **283**, 26312–26323.

Liang Q, Zhou B (2007) Copper and manganese induce yeast apoptosis via different pathways. *Mol. Biol. Cell* **18**, 4741–4749.

Luce K, Osiewacz HD (2009) Increasing organismal healthspan by enhancing mitochondrial protein quality control. *Nat. Cell Biol.* **11**, 852–858.

Ly JD, Grubb DR, Lawen A (2003) The mitochondrial membrane potential (deltapsi(m)) in apoptosis; an update. *Apoptosis* **8**, 115–128.

Marzetti E, Wohlgemuth SE, Lees HA, Chung HY, Giovannini S, Leeuwenburgh C (2008) Age-related activation of mitochondrial caspase-independent apoptotic signaling in rat gastrocnemius muscle. *Mech. Ageing Dev.* **129**, 542–549.

Matouschek A, Rospert S, Schmid K, Glick BS, Schatz G (1995) Cyclophilin catalyzes protein folding in yeast mitochondria. *Proc. Natl. Acad. Sci. U S A* **92**, 6319–6323.

Merlini L, Angelin A, Tiepolo T, Braghetta P, Sabatelli P, Zamparelli A, Ferlini A, Maraldi NM, Bonaldo P, Bernardi P (2008) Cyclosporin A corrects mitochondrial dysfunction and muscle apoptosis in patients with collagen VI myopathies. *Proc. Natl. Acad. Sci. U S A* **105**, 5225–5229.

Nakagawa T, Shimizu S, Watanabe T, Yamaguchi O, Otsu K, Yamagata H, Inohara H, Kubo T, Tsujimoto Y (2005) Cyclophilin D-dependent mitochondrial permeability transition regulates some necrotic but not apoptotic cell death. *Nature* **434**, 652–658.

Nicastro D, Frangakis AS, Typke D, Baumeister W (2000) Cryo-electron tomography of neurospora mitochondria. *J. Struct. Biol.* **129**, 48–56.

Osiewacz HD (1994) A versatile shuttle cosmid vector for the efficient construction of genomic libraries and for the cloning of fungal genes. *Curr. Genet.* **26**, 87–90.

Osiewacz HD (2002) Genes, mitochondria and aging in filamentous fungi. *Ageing Res. Rev.* **1**, 425–442.

Osiewacz HD, Borghouts C (2000) Cellular copper homeostasis, mitochondrial DNA instabilities, and lifespan control in the filamentous fungus *Podospora anserina*. *Exp. Gerontol.* **35**, 677–686.

Osiewacz HD, Esser K (1984) The mitochondrial plasmid of *Podospora anserina*: A mobile intron of a mitochondrial gene. *Curr. Genet.* **8**, 299–305.

Osiewacz HD, Skaletz A, Esser K (1991) Integrative transformation of the ascomycete *Podospora anserina*: identification of the mating-

type locus on chromosome VII of electrophoretically separated chromosomes. *Appl. Microbiol. Biotechnol.* **35**, 38–45.
Palma E, Tiepolo T, Angelin A, Sabatelli P, Maraldi NM, Basso E, Forte MA, Bernardi P, Bonaldo P (2009) Genetic ablation of cyclophilin D rescues mitochondrial defects and prevents muscle apoptosis in collagen VI myopathic mice. *Hum. Mol. Genet.* **18**, 2024–2031.
Pfaffl MW (2001) A new mathematical model for relative quantification in real-time RT-PCR. *Nucleic Acids Res.* **29**, e45.
Riddell RW (1950) Permanent stained mycological preparations obtained by slide culture. *Mycologia* **42**, 265–270.
Rizet G (1953) Sur l'impossibilité d'obtenir la multiplication ininterrompue et illimité de l'ascomycete *Podospora anserina*. *C R Acad. Sci. Paris* **237**, 838–855.
Savoldi M, Malavazi I, Soriani FM, Capellaro JL, Kitamoto K, da SilvaFerreiraME, Goldman MH, Goldman GH (2008) Farnesol induces the transcriptional accumulation of the *Aspergillus nidulans* Apoptosis-Inducing Factor (AIF)-like mitochondrial oxidoreductase. *Mol. Microbiol.* **70**, 44–59.
Scheckhuber CQ, Erjavec N, Tinazli A, Hamann A, Nyström T, Osiewacz HD (2007) Reducing mitochondrial fission results in increased life span and fitness of two fungal ageing models. *Nat. Cell Biol.* **9**, 99–105.
Scheckhuber CQ, Grief J, Boilan E, Luce K, Debacq-Chainiaux F, Rittmeyer C, Gredilla R, Kolbesen BO, Toussaint O, Osiewacz HD (2009) Age-related cellular copper dynamics in the fungal ageing model *Podospora anserina* and in ageing human fibroblasts. *PLoS ONE* **4**, e4919.
Schneider MD (2005) Cyclophilin D: knocking on death's door. *Sci. STKE.* **2005**, e26.
Semighini CP, Hornby JM, Dumitru R, Nickerson KW, Harris SD (2006) Farnesol-induced apoptosis in *Aspergillus nidulans* reveals a possible mechanism for antagonistic interactions between fungi. *Mol. Microbiol.* **59**, 753–764.
Stumpferl SW, Stephan O, Osiewacz HD (2004) Impact of a disruption of a pathway delivering copper to mitochondria on *Podospora anserina* metabolism and life span. *Eukaryot. Cell* **3**, 200–211.
Sun MG, Williams J, Munoz-Pinedo C, Perkins GA, Brown JM, Ellisman MH, Green DR, Frey TG (2007) Correlated three-dimensional light and electron microscopy reveals transformation of mitochondria during apoptosis. *Nat. Cell Biol.* **9**, 1057–1065.
Tropschug M, Barthelmess IB, Neupert W (1989) Sensitivity to cyclosporin A is mediated by cyclophilin in *Neurospora crassa* and *Saccharomyces cerevisiae*. *Nature* **342**, 953–955.
Vieira HL, Haouzi D, El HC, Jacotot E, Belzacq AS, Brenner C, Kroemer G (2000) Permeabilization of the mitochondrial inner membrane during apoptosis: impact of the adenine nucleotide translocator. *Cell Death Differ.* **7**, 1146–1154.
Zong WX, Thompson CB (2006) Necrotic death as a cell fate. *Genes Dev.* **20**, 1–15.
Zörnig M, Hueber A, Baum W, Evan G (2001) Apoptosis regulators and their role in tumorigenesis. *Biochim. Biophys. Acta* **1551**, F1–F37.

Supporting Information

Additional supporting information may be found in the online version of this article:

Fig. S1 Comparison of cyclophilin D from humans against the homologs of different aging models. ClustalW alignment of *P. anserina* CYPD (UniProt B2AAR4), *S. cerevisiae* CPR3 (UniProt P25719), *C. elegans* CYP1 (UniProt P52009), *D. melanogaster* CYP1 (UniProt P25007) and *H. sapiens* (human) CYPD (UniProt P30405). Black boxes indicate identical amino acids, gray boxes similar amino acids. A putative mitochondrial localization sequence (MitoProt) is marked by italic letters. All compared sequences are more than 44% identical to PaCYPD.

Fig. S2 *PaCypD* deletion. (a) Southern blot analysis with total DNA of the *PaCypD* deletion strain and the wild-type strain 's'. Hybridization with a *PaCypD* probe identified a band in wild-type DNA, while the *bsd*-probe, detecting the blasticidin gene of the bifunctional resistance cassette for selection and replacement, bound to DNA of the *PaCypD* deletion strain. (b) RT-PCR experiments with oligonucleotides, surrounding a part of *PaCypD* (251 bp), generate products with cDNA of wild-type as template but not with cDNA of the *PaCypD* deletion strain. Oligonucleotides, partly amplifying *PaPorin* (201 bp), were used for template control. Total DNA of wild-type strain 's' was used as template for the positive control (+). The larger PCR products are explained by an intron within the amplicons. In the negative control (–) water was used instead of template DNA. (c) generation of plDNA during aging is demonstrated in both the wild-type and the Δ*PaCypD* strain by Southern blot analysis. Total DNA of three juvenile (juv) and three senescent (sen) wild-type and Δ*PaCypD* strains were digested with *Bgl*II and hybridized with a probe corresponding to the intron 1 of the *Cox1* gene (plDNA probe). This region becomes amplified during aging, leading to the liberation of a 2.5 kb circular element (plDNA) visible as a 2.5 kb band. This goes along with a decrease in intact mtDNA (*Bgl*II-5 and *Bgl*II-17) normally detected as 1.9 and 5 kb fragments. Hybridization with the nuclear single-copy gene *Grisea* was used as a loading control.

Fig. S3 *PaCypD* overexpression. (a) Southern blot analysis with the overexpression plasmid pCypDEx1 and total DNA of wild-type and of the two overexpressing strains *PaCypD*_OEx1 and *PaCypD*_OEx2. A digoxigenin-labeled *PaCypD* probe was used for detecting the endogene, the transgene and the linearized overexpression plasmid. (b) Transcription level of *PaCypD* of juvenile wild-type (1, $n = 6$, dashed line), juvenile *PaCypD*_OEx1 (15.8 ± 3.2, $n = 6$, $P = 2.16E\text{-}3$) and juvenile *PaCypD*_OEx2 (11.7 ± 2.6, $n = 6$, $P = 2.16E\text{-}3$) determined by real-time PCR analysis. Expression was quantified relative to that of *PaPorin*. *PaCypD* expression is increased in juvenile *PaCypD*_OEx strains. (c) Generation of plDNA during aging is demonstrated in both the wild-type and the *PaCypD* overexpressing strain by Southern blot analysis. Comparing 9-day-old *PaCypD*_OEx strains with 18-day-old wild-type strains revealed the same strong plDNA accumulation in the *PaCypD* overexpressing strains demonstrating a faster aging process. Hybridization with the nuclear single-copy gene *Grisea* was used as a loading control.

Fig. S4 Protein level of PaHSP60 visualized by Western blot analysis and densitometry using mitochondrial protein extracts from juvenile wild-type strain 's' ($n = 3$), senescent wild-type ($n = 3$) and juvenile *PaCypD*_OEx cultures ($n = 3$). Predicted

sizes of the proteins are indicated on the right. The PaHSP60 levels of juvenile wild-type mitochondria (1 ± 0.17), senescent wild-type mitochondria (1.49 ± 0.33; P = 1E-1) and juvenile *PaCypD*_OEx mitochondria (1.46 ± 0.42; P = 1E-1) do not differ significantly. PaPORIN was used as loading control for quantification.

Fig. S5 Senescence markers in the *PaCypD* overexpressing strains. (a) Transcription level of *PaMt1* of juvenile wild-type strain 's' (1, n = 6, dashed line), juvenile *PaCypD*_OEx1 (5.9 ± 1.3, n = 6, P = 2.16E-3) and juvenile *PaCypD*_OEx2 (5.8 ± 2.6, n = 6, P = 2.16E-3) was determined by real-time PCR analysis. Expression was quantified relative to the *PaPorin* expression. *PaMt1* expression is increased in juvenile *PaCypD*_OEx strains. (b) Transcription level of *PaSod2* of juvenile wild-type strain 's' (1, n = 6, dashed line), juvenile *PaCypD*_OEx1 (1.27 ± 0.23, n = 6, P = 1) and juvenile *PaCypD*_OEx2 (0.74 ± 0.2, n = 6, P = 1) was determined by real-time PCR analysis. Expression was quantified relative to the *PaPorin* expression. *PaSod2* expression in juvenile *PaCypD*_OEx strains is comparable to juvenile wild-type cultures. (c) Determination of PaSOD2 activity in juvenile, middle-aged and senescent wild-type and *PaCypD*_OEx strains. While wild-type strains display no PaSOD2 activity only in the senescent stage, already in juvenile *PaCypD* overexpressing strains PaSOD2 activity was absent.

Table S1 Oligonucleotides used for RT-PCR and real-time PCR analysis. The used primer pairs amplify a selected region of one gene containing an intron. This explains the different product sizes depending on the used template.

Table S2 Statistical analysis of lifespan data in Fig. 1 by Log Rank (Mantel-Cox), Breslow (Generalized Wilcoxon), Tarone-Ware and Wilcoxon (two-tailed). (a) Lifespan of the Δ*PaCypD* strain is not significantly changed compared to wild-type. (b) The statistical tests indicate that lifespan of the two overexpressors *PaCypD*_OEx-T1 and *PaCypD*_OEx-T2 is significantly decreased.

Table S3 Statistical analyses of lifespan data in Fig. 4 by Log Rank (Mantel-Cox), Breslow (Generalized Wilcoxon), Tarone-Ware and Wilcoxon (two-tailed). (a) Treatment with 0.02 μg mL^{-1} CSA influences wild-type lifespan positively. (b) Treatment with 0.1 μg mL^{-1} CSA leads to a significant lifespan increase in 6-day-old wild-type cultures. (c) CSA treatment of *PaCypD*_OEx strains changed lifespan significantly compared to untreated *PaCypD*_OEx strains. 0.02 und 0.04 μg mL^{-1} CSA influence *PaCypD*_OEx Lifespan positively, 0.1 μg mL^{-1} leads to a dramatic lifespan decrease. (d) Lifespan of the Δ*PaCypD* strain is not influenced by CSA treatment.

Table S4 Raw data of the survival analyses shown in Fig. 1. Age intervals in days; number entering the age interval (Nx); Number of dead inoculates within the age interval (dx); Number censored within the age interval (cx).

Table S5 Raw data of the survival analyses shown in Fig. 4. Age intervals in days; number entering the age interval (Nx); Number of dead inoculates within the age interval (dx); Number censored within the age interval (cx).

As a service to our authors and readers, this journal provides supporting information supplied by the authors. Such materials are peer-reviewed and may be re-organized for online delivery, but are not copy-edited or typeset. Technical support issues arising from supporting information (other than missing files) should be addressed to the authors.